25·29 August 2024
inter.noise
NANTES FRANCE

Analysis of a brake squeal functional model using a linear parameter varying perspective.

Guilherme MALACRIDA ALVES[1]
PIMM, Arts et Metiers institute of technology, CNRS, Cnam, HESAM / SDTools
151 Bd. de l'Hôpital, 75013 Paris, France / 44 rue Vergniaud, 75013 Paris, France

Etienne BALMES[2]
PIMM, Arts et Metiers institute of technology, CNRS, Cnam, HESAM / SDTools
151 Bd. de l'Hôpital, 75013 Paris, France / 44 rue Vergniaud, 75013 Paris, France

Guillaume MARTIN[3]
SDTools
44 rue Vergniaud, 75013 Paris, France

ABSTRACT

Brake squeal is a limit cycle vibration induced by mode coupling instability that depends on operating conditions such as applied pressure, temperature, and disk velocity. This work proposes a simplified functional model of brake squeal that reproduces the main characteristics observed in a full-scale industrial test campaign: vibration growth, limit cycle saturation, vibration decay and parametric dependence. The proposed functional model differs from the well-known Hoffmann model by the introduction of a nonlinear contact law and a quasi-static pressure loading. First, using a harmonic balance perspective, non-linear forces are shown to lead to a pressure and amplitude dependent contact stiffness. This Linear Parameter Varying perspective allows complex mode computations in the pressure/amplitude domain which are then correlated with a series of transient responses of the nonlinear modes for three different pressure profiles. The chosen profiles represent usual experiments: drag where a constant pressure is applied, pressure ramps and pressure oscillations mimicking the effect of wheel spin on the contact surfaces.

1. INTRODUCTION

Brake squeal a common industrial problem characterized by a self excited vibration induced by a mode a coupling instability. Due to the nonlinear nature of brake systems the presence of squeal is dependent on the system operating conditions such as applied pressure, temperature, and disk velocity. The characterization of brake squeal consists in identifying the range of operating conditions for which squeal occurs and describing the resulting limit cycle vibration. Experimental measurements [1] have shown that some parametric effects cannot be eliminated in a practical case such as the changes in contact stiffness induced by the wheel angular position.

[1]guilherme.malacrida_alves@ensam.eu

[2]etienne.balmes@ensam.eu

[3]martin@sdtools.com

Taking this into consideration this paper seeks to represent the changes induced by slow pressure variations in a simplified functional model.

In order to describe the mechanism behind the mode coupling instability Hoffmann [2] proposed an simple two degrees of freedom model that describes the formation of instability as a function of the friction coefficient μ. An alternative approach was proposed by Meehan [3] for describing the wheel-rail squeal phenomenon and later adapted to brake squeal [4] points out that spragging is a necessary condition for the presence of stiffness mode coupling instability. However due to the transposition of the model between domains some geometric considerations on the direction of the contact forces relative to the mode shapes that are less clear on the case of a pad-disk than on wheel-rail contact. In [5, 6] the influence of the equilibrium position in the occurrence of squeal is studied. The effect of vibration amplitude on the system is evaluated in [7] by considering a trajectory that follows the shape of the unstable mode. This approach has the interesting characteristic of being able to estimate for which amplitude a poles ceases to be unstable and forms a limit cycle.

In section 2 a modification of the functional model proposed by [2] is proposed. The proposed functional model is composed of two degrees of freedom system subject to contact and friction nonlinearities. This model is able to represent the mode coupling instability, limit cycle saturation and parametric changes due to operating conditions. The parametric effects being induced by an external slow varying load mimicking the pressure applied by the piston in a brake system.

Section 3 looks at two different ways of constructing a linear parameter varying (LPV) model from the proposed nonlinear model. First the well known tangent linearization computed around the static sliding equilibrium as a function of the external load. The second linearization is done by introducing a periodic trajectory on the system and projecting the nonlinear forces in the first harmonic. The result is an equivalent stiffness chart that is a function of both the applied pressure and vibration amplitude similar to what can be obtained using nonparametric identification of localized nonlinearities [8]. Using these two linearizations a series of eigenvalue analysis is performed estimating the unstable operating conditions, limit cycle amplitude and the changes in mode shape induced by vibration amplitude.

The last section 4 comes back to the end objective of this study that is to provide a reference that can be used to validate experimental strategies [9]. Transient simulations of usual experiments: drag where constant pressure is applied, pressure ramps, and pressure oscillations mimicking the contact changes due to wheel spin, which the authors think is the source of intermittent squeal occurrences. The transients reproduce stability boundaries, limit cycle saturation, sensitivity to pressure. Relation with the proposed LPV models depending on static pressure and amplitude is discussed. It is show the that the LPV analysis restricted to first harmonic is sufficient to reproduce stability boundaries and limit cycle amplitude dependence to pressure.

2. MODEL DEFINITION

The proposed functional model, shown in figure 1, is a two degrees of freedom system with a linear portion composed of a mass held by two orthogonal spring-damper pairs. This is meant to represent the two modes interacting in a break squeal situation. A contact and friction nonlinearity is introduced by a sliding plane at an angle θ and couples the two with loads normal F_{NOR} and tangent F_{TAN} to the sliding plane. For simplicity the interaction on the contact surface is considered to be at a single point, in more detailed reduced brake models a pressure distribution over the contact surface is considered.

In [4] the contact angle θ (also called the sprag angle) is related to the spragging condition a necessary condition for stiffness mode coupling. That is, stiffness mode coupling can only occur when $0 < \tan(\theta) < \mu$ where μ is the friction coefficient. A more detailed evaluation of the conditions

for stability is described in [4].

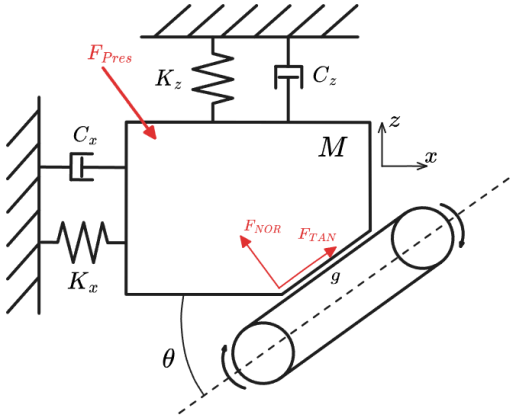

Figure 1: Lumped elements diagram of the proposed 2-DoF functional model

The differential equation describing this model is

$$\underbrace{\begin{bmatrix} M & 0 \\ 0 & M \end{bmatrix}}_{[M]} \begin{Bmatrix} \ddot{x} \\ \ddot{z} \end{Bmatrix} + \underbrace{\begin{bmatrix} C_x & 0 \\ 0 & C_z \end{bmatrix}}_{[C]} \begin{Bmatrix} \dot{x} \\ \dot{z} \end{Bmatrix} + \underbrace{\begin{bmatrix} K_x & 0 \\ 0 & K_z \end{bmatrix}}_{[K]} \begin{Bmatrix} x \\ z \end{Bmatrix} + \left\{\tilde{F}_{NOR}(x,z)\right\} + \left\{\tilde{F}_{TAN}(x,z)\right\} - \left\{\tilde{F}_{Pres}\right\} = 0 \quad (1)$$

An external load $\tilde{F}_{Pres}$ is applied to represent the pressure applied on the brake system. This force is considered static, or slowly varying (quasi-static) so that it can play the role of operating condition (external parameter).

$$\left\{\tilde{F}_{Pres}\right\} = \begin{bmatrix} -\sin(\theta) \\ +\cos(\theta) \end{bmatrix} F_{Pres}(t_{slow}) = \left[\tilde{b}_{Pres}\right] F_{Pres}(t_{slow}) \quad (2)$$

The normal part of the nonlinear force represents the contact nonlinearity. Where the term $P_c(-g)$ represents the nonlinear contact law as a function of $-g$ the overclosure, penetration, or opposite of the gap between surfaces. For a simplicity of notation the overclosure $-g$ is going to be noted as g throughout this paper. g that plays the role of contact strain is linearly related to DOF by the observation equation $g = [\tilde{c}_{NOR}]\{q\}$. The key aspect for the contact law is that it is assumed to be amplitude dependent, and thus not piecewise linear, which is verified for surfaces that are not considered ideally flat [10]. In this study the exponential contact law used by Hitachi Astemo is retained

$$P_c(g) = p_z e^{\lambda(g)} \quad (3)$$

For a given pressure the forces applied on the system DOF is found

$$\left\{\tilde{F}_{NOR}\right\} = S_{pad} \begin{bmatrix} \sin(\theta) \\ -\cos(\theta) \end{bmatrix} P_c(g) = \left[\tilde{b}_{NOR}\right] P_c(g) \quad (4)$$

The tangent part of the force represents the Coulomb friction nonlinearity under constant sliding. The friction coefficient μ is in some cases considered to be dependent on the magnitude of the sliding velocity ([4] for example), for the scope of this study however it will be considered to be constant to emphasize the fact that friction dependence is not necessary to explain

the limit cycle properties. Similarly to the contact force, F_{TAN} can then be described using observation/command formalism as

$$\{\tilde{F}_{TAN}\} = -\mu S_{pad} \begin{bmatrix} \cos(\theta) \\ \sin(\theta) \end{bmatrix} P_c(g) = -\mu \left[\tilde{b}_{TAN}\right] P_c(g) \tag{5}$$

Taking a linear system reference, it is then possible construct a set of modal coordinates $\{q\} = [\phi] \begin{Bmatrix} x \\ z \end{Bmatrix}$ such that $[\phi]^T [M] [\phi] = [I]$ and $[\phi]^T [K] [\phi] = \left[\backslash \omega_{j\backslash}^2\right]$. By using the modal coordinate transformation and substituting the expressions of loads Equation 2, Equation 3 and Equation 5 into Equation 1, we obtain the nonlinear dynamic equation for the functional model, one obtains equations in modal coordinates where

$$[I] \{\ddot{q}\} + \left[\backslash 2\zeta_j \omega_{j\backslash}\right] \{\dot{q}\} + \left[\backslash \omega_{j\backslash}^2\right] \{q\} + \left[b_{NOR} - \mu b_{TAN}\right] P_c\left([c_{NOR}] \{q\}\right) - [b_{Pres}] F_{Pres} = 0. \tag{6}$$

where $b_{NOR} = [\phi]^T \left[\tilde{b}_{NOR}\right]$, $c_{NOR} = [\tilde{c}_{NOR}] [\phi]$, $b_{TAN} = [\phi]^T \left[\tilde{b}_{TAN}\right]$ and $b_{Pres} = [\phi]^T \left[\tilde{b}_{Pres}\right]$.

Although the representation of a brake system through a simple functional model may seen restrictive in a first glance, a similar development can be applied to a two mode reduced model resulting from the linearization of a full brake finite element model. This does not come without its share if difficulties as dealing with the varying levels of contact pressure across the contact surface and their dependence to parameters may prove to be a challenge and are beyond the scope of this paper. The values shown in table 1 where selected manually to be somewhat close to experimental results.

Table 1: Parameters chosen for the functional squeal model

m [kg]	ω_x [kHz]	ω_z [kHz]	ζ_x [%]	ζ_z [%]	p_z [MPa]	λ $[mm^{-1}]$	θ [^{o}]	S_{Pad} $[mm^2]$
1	1.5	1.45	0.1	0.2	0.01	750	25	20

3. LINEARIZATION AND COMPLEX EIGENVALUE ANALYSIS (CEA)

Two different linearization strategies are considered in this paper for the construction of a linear parameter varying eigenvalue problem. The goal of this eigenvalue analysis is to evaluate the poles evolution and describe the presence and evolution of instability under specific operating condition. First using a tangent linearization to describe the nonlinear contact as a funtion of the applied pressure and then building an equivalent stiffness that depends on both applied pressure and vibration amplitude.

3.1. Tangent linearization

In this first step the system dynamics is linearized a around a static operating condition with constant sliding. The static response of the system to an external load F_{Pres} is described by Equation 7 and results in a static displacement $\{q_0\}$, inducing a static overclosure $g_0 = [c_{NOR}] \{q_0\}$ that can be obtained analytically.

$$\left[\backslash \omega_{j\backslash}^2\right] \{q_0\} + \left[b_{NOR} - \mu b_{TAN}\right] P_c\left([c_{NOR}] \{q_0\}\right) - [b_{Ext}] \{F_{Ext}\} = 0. \tag{7}$$

The nonlinear contact law is then linearized around g_0. Thus a first order approximation of pressure $P_c(g) \approx K_c(g_0) [c_{NOR}] \left(\{q\} - \{q_0\}\right)$ leads to

$$K_c(g_0) = \frac{\partial P_c}{\partial (g)}(g_0) = p_z \lambda e^{\lambda g_0} \tag{8}$$

As a mean of establishing a notion of scale for the contact stiffness, it is displayed relative to $K_x = m\omega_x^2$. In the considered range of F_{Pres} (from $250N$ to $550N$) the value of K_c/K_x is between 2 and 20%, while the difference between $K_z = m\omega_z^2$ and K_x is around 6.5%.

By replacing Equation 8 into Equation 6 the system becomes linear and a complex eigenvalue problem depdendent on g_0 is found

$$\left(\lambda^2 [I] + \lambda \left[\backslash 2\zeta_j \omega_{j\backslash}\right] + \left[\backslash \omega_{j\backslash}^2\right] + \left[b_{NOR} - \mu b_{TAN}\right] K_c(g_0) [c_{NOR}]\right)\{\psi\} = 0 \tag{9}$$

Each of the resulting poles $\lambda_j = -\zeta_j \omega_j + i\omega_j \sqrt{1-\zeta_j^2}$ is unstable if its real part is positive or its damping coefficient ζ_j negative. In classical Linear Time Invariant (LTI) analysis, the system is considered unstable if at least one pole is unstable.

The choice to consider F_{Pres} as a parameter instead of the friction coefficient μ as in [2] was made to include the nonlinear contact law in the stability analysis. Thus the effects of changes in pressure changes correspond to a Linear Parameter Varying (LPV) evolution. As shown in figure 2 in the case of the considered functional system, the CEA lets us evaluate the range of static load for which the system is unstable.

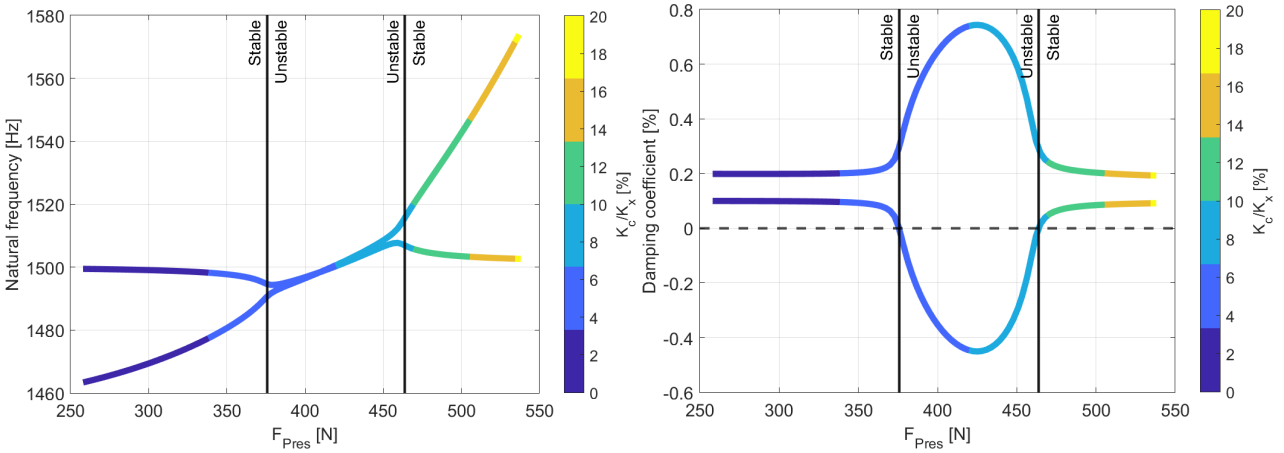

Figure 2: Evolution of the linearized system poles as a function of the static load F_{pres}. Left: natural frequency. Right: damping coefficient.

This first linearization considered that the displacement around the static equilibrium is small enough that higher order contributions can be ignored. As soon as the system enters the unstable region, this condition fails and the linearization is no longer valid, resulting in a inability to predict limit cycle stabilization and final amplitude.

3.2. Linearization around a periodic trajectory

The second approach considered here seeks to include an amplitude dependence in the eigenvalue problem Equation 9 in order to describe both limit cycle vibration and the effects of operating conditions. The works of [7, 11] use the modal amplitude as a parameter in the construction of amplitude dependent eigenvalue problems. By considering the modal amplitude as a parameter these works assume that the vibration follows a periodic harmonic trajectory following the corresponding mode shape which allow the construction of an equivalent dynamic stiffness. A non parametric approach to describing the construction of dynamic system is described in [8].

Keeping the same ideas in mind, a periodic trajectory of the overclosure composed of harmonics 0 (static) and 1 $g(g_0, g_1, t) = Re\left(g_0 + g_1 e^{i\omega t}\right)$ is used. This parametrization corresponds

to the description of the solution using g_0, g_1, ω as unknowns, which the basis of the harmonic balance method (HBM) [12–14]. The HBM formulates equilibrium in a weak sense over one period. An equivalent stiffness $K_c(g_0, g_1)$ is thus defined by choosing the value giving the same work as the non-linear forces for the assumed gap trajectory. In other words

$$R_1(\omega) = \int_0^{2\pi/\omega} P_c(g(t))e^{-i\omega t}dt = K_c(g_0, g_1)\int_0^{2\pi/\omega} g(t)e^{-i\omega t}dt = K_c(g_0, g_1)g_1\frac{2\pi}{\omega} \tag{10}$$

leading to the equivalent stiffness

$$K_c(g_0, g_1) = \frac{\int_0^{2\pi/\omega} P_c(g(t))e^{-i\omega t}dt}{\int_0^{2\pi/\omega}(g(t))e^{-i\omega t}dt} = \frac{F_1(g_0, g_1)}{g_1} \tag{11}$$

This approach is similar to the non parametric identification used in [8]. Note that the imposed periodic trajectory of g means that the static component of the contact pressure P_{c0} is also dependent on g_1.

$$\left(\lambda^2[I] + \lambda\left[\backslash 2\zeta_j\omega_j\backslash\right] + \left[\backslash\omega_j^2\backslash\right] + \left[b_{NOR} - \mu b_{TAN}\right]K_c(g_0, g_1)\left[c_{NOR}\right]\right)\{\psi\} = 0 \tag{12}$$

Following the definition in Equation 11, figure 3 displays the dependence of K_c relative to $K_x = m\omega_x^2$ as a function of g_1 and F_{pres} (related to g_0 by the non-linear static problem in Equation 7). Figure 3 also displays the root locus as a function of $K_c(g_0, g_1)$. As the equivalent stiffness is a scalar value, the path of the poles in figure 3 is the same as the one displayed in figure 2 but as a function of F_{pres} and g_1 instead of only F_{pres}.

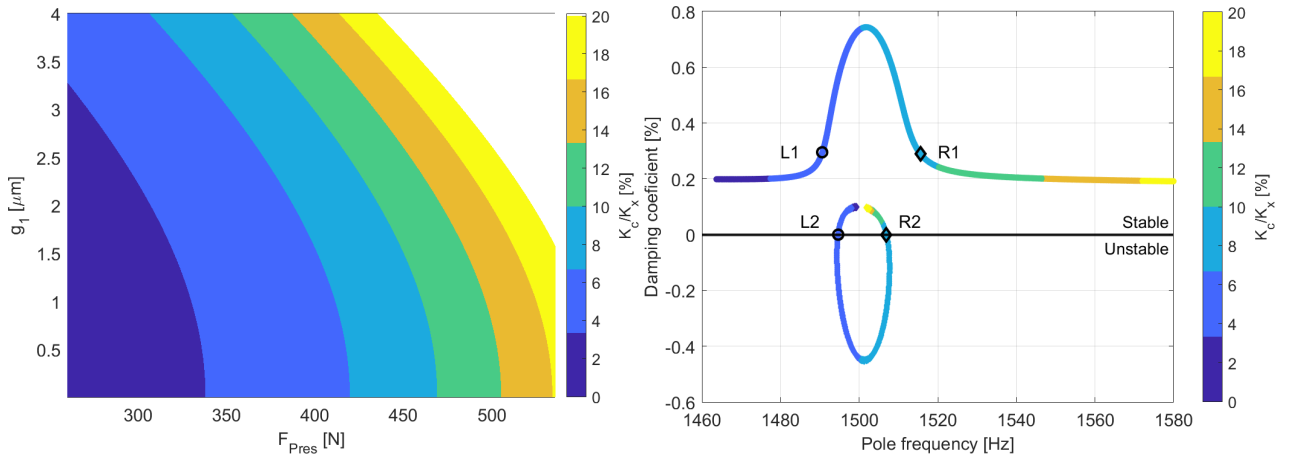

Figure 3: Left: Equivalent stiffness evolution with the static load F_{pres} and first harmonic amplitude g_1. Right: Poles obtained from Equation 9 for different values of contact stiffness K_c (Root Locus). Pairs of poles corresponding to the crossing of the $\zeta = 0$ (limit cycles) are indicated by L1/L2 and R1/R2.

From the obtained poles it is then possible to trace the evolution of ζ for the unstable pole in the g_0, g_1 parametric space (figure 4). Positive damping areas left and right are stable. In the middle, an unstable region cannot correspond to a limit cycle (stable periodic solution) as negative damping leads to amplitude growth. Physically possible limit cycles, a constant but non small harmonic 1, are located at the boundary where zero damping as a result of an amplitude dependent eigenvalue analysis [7, 11]. Thus showing that this functional model represents the saturation mechanism that sufficiently changes the system to stop vibration from growing.

In order to take a closer look at the saturation mechanism, we analyze the evolution of the mode shapes $\{\psi_j(g_0, g_1)\}$ obtained from Equation 12 with g_1 for a fixed static load $F_{pres} = 400N$ using the modal assurance criterion (MAC).

$$MAC(\psi_a, \psi_b) = \frac{|\psi_a^T \psi_b|^2}{\|\psi_a\|^2 \|\psi_b\|^2} \tag{13}$$

Taking the mode shapes at $g_1 = 0$ as a reference figure 4 shows the evolution of the MAC with g_1. It is noticeable that as g_1 increases the mode shapes of both the stable and unstable mode slowly change resulting in a decreasing MAC value until reaching the stability boundary. The g_1 value at the stability boundary represents the first harmonic amplitude where a limit cycle vibration is possible under the given operating conditions. Further increasing the amplitude g_1 results in the MAC for the stable pole increasing while for the unstable pole it continues to decrease. The main conclusion from this is that changes in complex mode shape have an important effect in the formation of a limit cycle. This shape evolution with vibration amplitude is something that has been noted in [15] for the case of bolted assemblies.

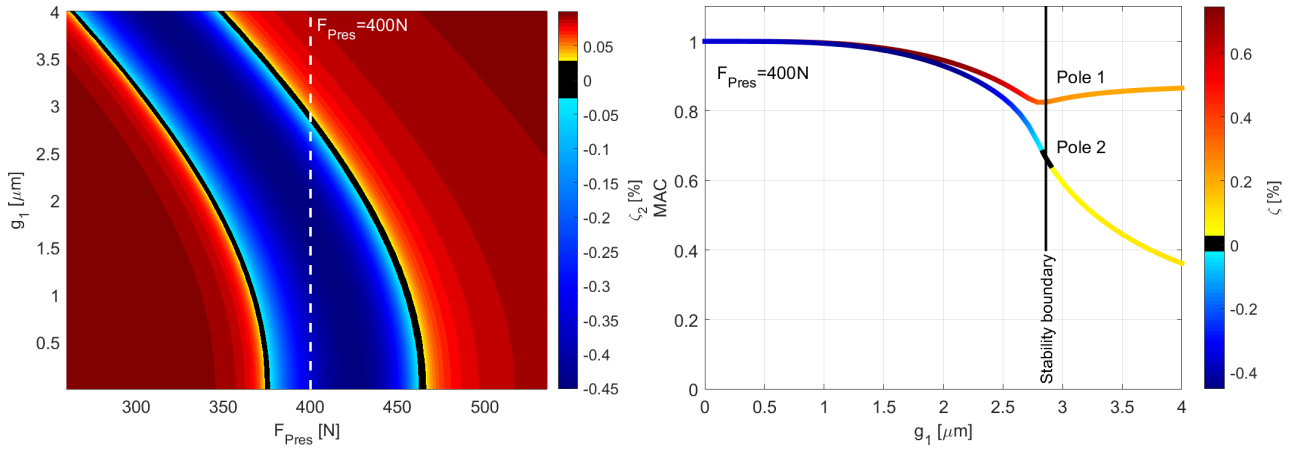

Figure 4: Left: Damping coefficient of the unstable mode ζ_2 evolution with the static load F_{Pres} and first harmonic amplitude g_1. LPV stability boundary shown as black line. Vertical white line indicating $F_{Pres} = 400N$. Right: Evolution of the MAC between mode shapes of the stable and unstable poles as a function first harmonic amplitude g_1 for $F_{Pres} = 400N$ with ζ indicated as color. Vertical line indicate the amplitude corresponding to $\zeta_2 = 0$ (limit cycle).

4. COMPARING TRANSIENT SIMULATION WITH EIGENVLAUE PREDICTIONS

Next we evaluate the nonlinear system response in time domain using transient simulation computed with a modal Newmark nonlinear scheme [16]. In the transient simulations the a slowly varying external force F_{Pres} is applied to the system with small background noise that allows visualization of modes in stable regions and is found physically due to irregularities of the sliding surfaces.

Three different force profiles are considered in this section in order to display the different conditions we seek to evaluate brake. First the limit cycle formation under a constant static load is evaluated. Followed by two profiles that seek to characterize the parametric variations of the system: a slow ramp in F_{Pres} passing through the unstable region and a periodic oscillation that enter and exits the unstable region.

4.1. Constant static load

In this first test we seek to evaluate the limit cycle formation by applying the force profile depicted in figure 5 left. The applied pressure F_{Pres} slowly raises from zero until $370N$ close to the unstable region (see figure 4), stabilizes for $0.4s$ to limit remaining transient effects from the initial load and then increases to $385N$ triggering the instability. In 5 right it is possible to see the static response

slowly evolving with near zero vibration until the system enters the unstable region, where the vibration amplitude suddenly increases and quickly reaches a limit cycle that remains stable until the end of the simulation. This shows that the proposed model is capable of reproducing the mechanisms responsible for unstable growth and limit cycle formation.

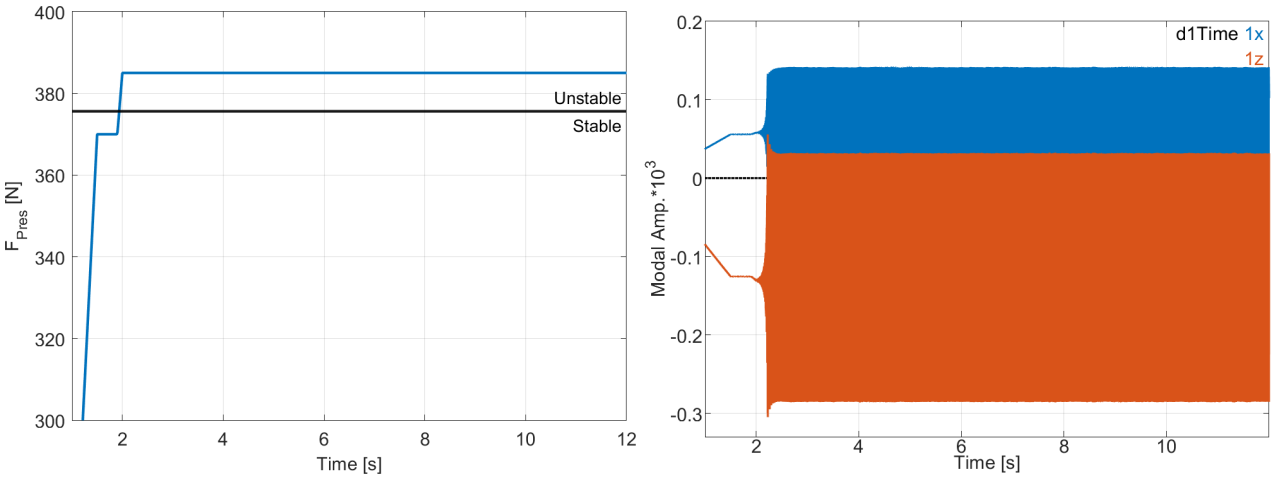

Figure 5: Left: Constant static load F_{Pres} profile and stability frontier. Right: Modal amplitudes evolution over time

4.2. Slow ramp static load

In this second analysis the limit cycle dependence to the applied pressure is evaluated by slowly increasing the applied pressure. Such pressure ramps are considered in real tests. The value of $g_1(t)$ is then extracted using synchronuous demodulation [9, 17] and then shown in figure 6. It is very clear that as soon as the system enters in unstable range the gap vibration amplitude rapidly increases until reaching a saturation where amplitude now change slowly with the applied pressure until re-entering the stable region. The superposition between of the estimated limit cycle from the eigenvalue analysis (figure 4) with the first harmonic from the transient response shows that g_1 follows closely the predicted limit cycle.

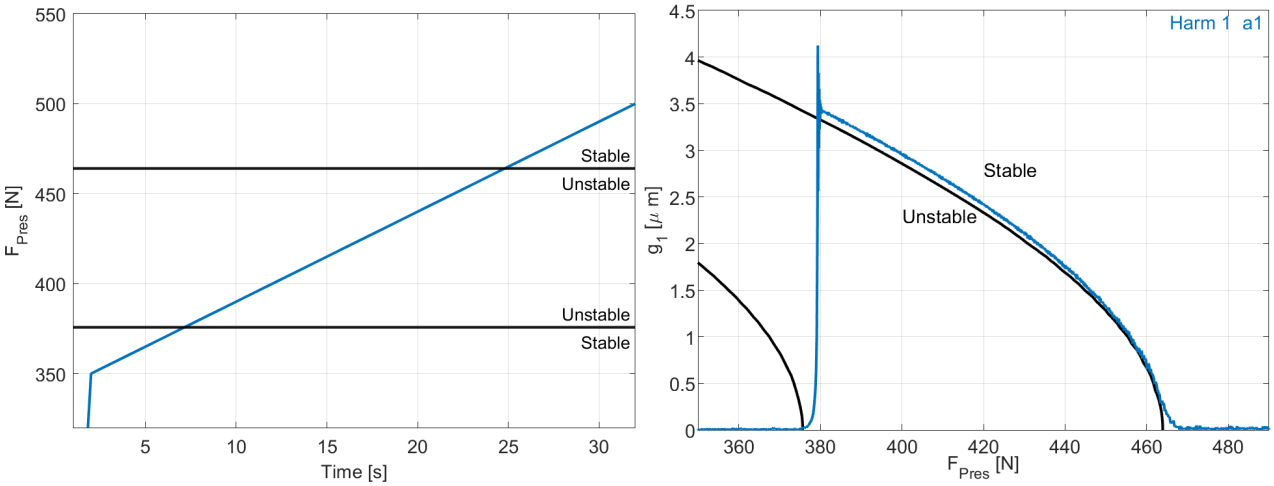

Figure 6: Left: Slow ramp static load F_{Pres} profile and stability frontier. Right: First harmonic component of the overclosure $g_1(t)$ extracted using demodulation (blue) and LPV stability boundary (black) as a function of F_{Pres}.

By combining the extracted value of g_1 with the applied F_{pres} and the results from the eigenvalue analysis (figures 3 and 4) it is possible to estimate the system poles under this operating conditions. Figure 7 compares these estimated poles with the spectrogram of the overclosure g obtained in the transient simulation, where it can be seen that the limit cycle frequency match with the frequency predicted in the eigenvalue analysis (pole R2 in figure reff:stif-rlocus). As there is a small level of noise added in the simulation it is also possible to see the response of the system modes before and after the unstable region.

The spectrogram also shows the presence of sidebands around the limit cycle that starts at around double the distance between estimated poles and slowly gets closer. This as well as the amplitude difference between limit cycle amplitude and stability boundary (figure 6) may be caused by a number of reasons such as the presence higher harmonics not considered in the eigenvalue analysis, the numerical integration scheme or the added noise to the system.

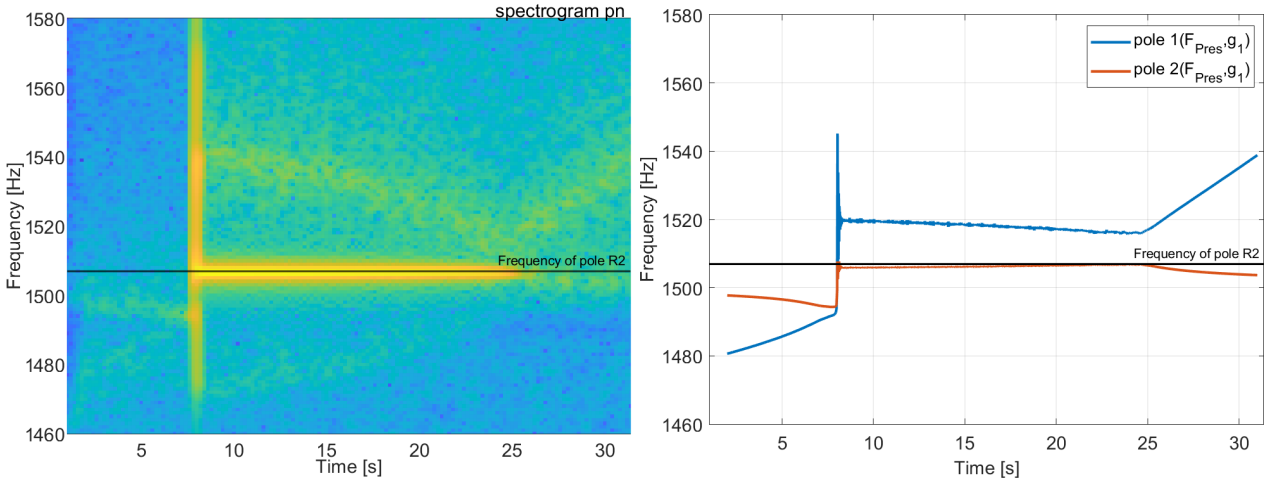

Figure 7: Left: Spectrogram of the overclosure g at the contact interface. Right: Evolution of the natural frequency of poles interpolated from figure 3 using the trajectory of F_{Pres}, g_1 from the transient simulation.

4.3. Oscillating static load

Lastly, by using a oscillating external force (figure 8) a intermittent squeal is induced in the system. This imitates the periodic parametric variations induced for example by changes related to the angular position that is observed in practical cases [1].

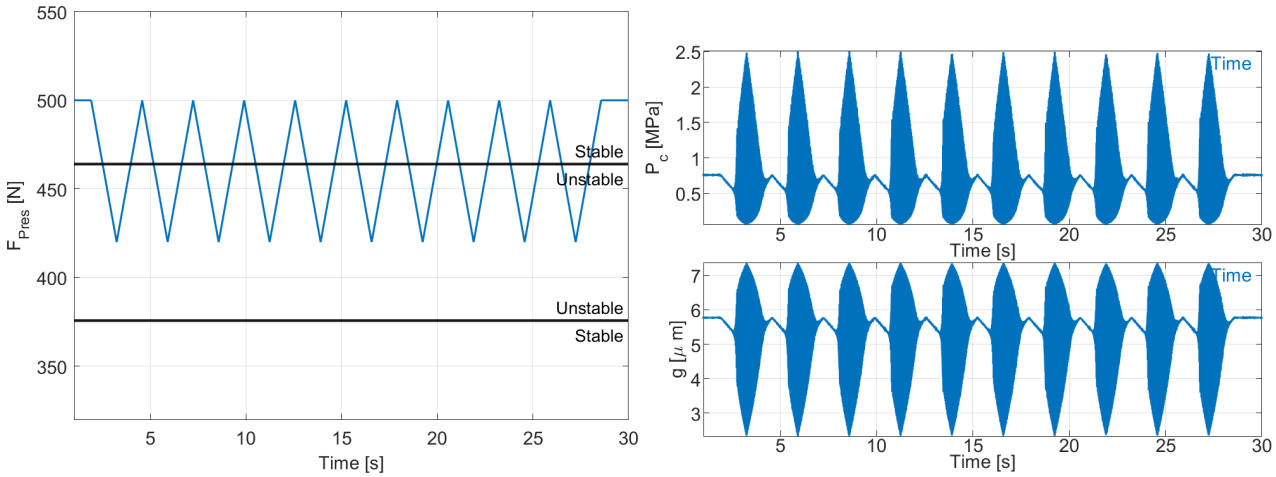

Figure 8: Left: Oscillating static load profile F_{Pres} profile and stability frontier. Right: Overclosure g and contact pressure P_c evolution over time.

By once again plotting the extracted first harmonic g_1 as function of F_{Pres} in figure 9, it is possible to see that the induced vibration is repeatable and that there is a difference in the path between entering and exiting the unstable region. Following the evolution of g_1 in the left part of figure 9 starting at $F_{Pres} = 500N$ at $g_1 = 0$ with time (color) it is possible to see that after crossing the stability boundary g_1 starts to increase. At first the characteristic time of the parametric variation is faster then the characteristic time of the vibration growth and vibration cannot follow this frontier. As pressure continues to fall the values of F_{Pres}, g_1 evolve inside the unstable region leading to a increase in growth rate, which combined with a slower parametric variation leads to g_1 catching up to the stability frontier. The vibration amplitude then follows the stability boundary as pressure decreases and increases until parametric variations gets faster once again near the limit of the unstable range of F_{Pres}. At this point the characteristic time of the system dissipation is slower than the variations of the stability boundary amplitude leading to a remaining vibration that is slowly dissipated. This behavior is repeated in all pressure oscillations as shown in the right part of figure 9. The difference is behavior when crossing the stability boundary in both senses is caused by the low growth and damping rates present near the stability boundary, which indicates that parametric studies using transient simulations or experimental measurements should be careful to ensure the parametric changes are sufficiently slow in order to accurately characterize parametric effects.

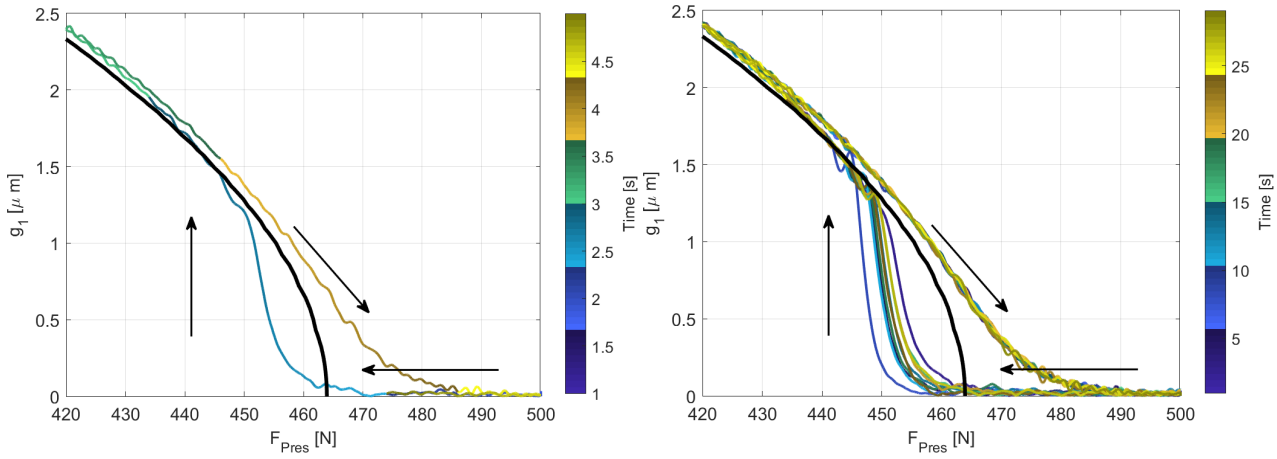

Figure 9: Evolution of the first harmonic of the overclosure g_1 as a function of F_{Pres} and time (color) compared to the LPV stability boundary (black). Arrows indicating the sense of time evolution. Left: first 5 s Right: complete simulation.

5. CONCLUSION AND PERSPECTIVES

In this paper we have proposed a modification of the functional model proposed by [2] in order to represent the changes induced by slow pressure variations representative of an experimental parametric measurement. In particular this model is able to provide an insight into a series of usual experiments such as : drag where constant pressure is applied, pressure ramps, and pressure oscillations mimicking the contact changes due to wheel spin. The combination of the transient analysis from section 4 with the LPV eigenvalue analysis from 3 provides a basis for designing and validating experimental strategies used to characterize the parametric dependencies of brake squeal on operating condition. This allows a better design of experiments aimed to characterize the mechanisms inducing mode coupling instability, limit cycle saturation or parametric changes on vibration amplitude. Additionally these ideas may serve as a guideline for the development of model updating strategies that correlate measured and estimated parametric changes leading to the construction of predictive reduced industrial models.

ACKNOWLEDGEMENTS

We wish to thank ANRT, and Hitachi Astemo for their contribution to funding the first author's thesis.

REFERENCES

1. Guillaume Martin, Etienne Balmes, Guillaume Vermot Des Roches, and Thierry Chancelier. Squeal measurement using operational deflection shape. Quality assessment and analysis improvement using FEM expansion. In *Eurobrake*, 2017.
2. N. Hoffmann and L. Gaul. Effects of damping on mode-coupling instability in friction induced oscillations. *ZAMM*, 83(8):524–534, August 2003.
3. Paul A. Meehan. Prediction of wheel squeal noise under mode coupling. *Journal of Sound and Vibration*, 465:115025, January 2020.
4. Paul A. Meehan and Andrew C. Leslie. On the mechanisms, growth, amplitude and mitigation of brake squeal noise. *Mechanical Systems and Signal Processing*, 152:107469, May 2021.
5. Sebastian Koch, Holger Gödecker, and Utz von Wagner. On the interrelation of equilibrium positions and work of friction forces on brake squeal. *Archive of Applied Mechanics*, 92(3):771–784, March 2022.
6. Sebastian Koch, Nils Gräbner, and Utz von Wagner. A minimal model for the influence of equilibrium positions on brake squeal. *GAMM-Mitteilungen*, 46(1):e202300001, 2023.
7. S. Nacivet and J.-J. Sinou. Modal Amplitude Stability Analysis and its application to brake squeal. *Applied Acoustics*, 116:127–138, January 2017.
8. Taylan Karaağaçlı and H. Nevzat Özgüven. A frequency domain nonparametric identification method for nonlinear structures: Describing surface method. *Mechanical Systems and Signal Processing*, 144:106872, October 2020.
9. Guilherme Malacrida Alves, Etienne Balmes, Guillaume Martin, Guillaume Vermot Des Roches, Deyuan Zhang, and Thierry Chancelier. An harmonic balance vector signal model to study slow parametric sensitivity of brake squeal occurrences. *MSSP*, Submitted to, 2023.
10. L. Pesaresi, J. Armand, C.W. Schwingshackl, L. Salles, and C. Wong. An advanced underplatform damper modelling approach based on a microslip contact model. *Journal of Sound and Vibration*, August 2018.
11. Taylan Karaağaçlı and H. Nevzat Özgüven. Experimental modal analysis of nonlinear systems by using response-controlled stepped-sine testing. *Mechanical Systems and Signal Processing*, 146:107023, January 2021.

12. Mikhail Guskov and Fabrice Thouverez. Harmonic Balance-Based Approach for Quasi-Periodic Motions and Stability Analysis. *Journal of Vibration and Acoustics*, 134(031003), April 2012.
13. Vincent Jaumouillé, Jean-Jacques Sinou, and Benoît Petitjean. An adaptive harmonic balance method for predicting the nonlinear dynamic responses of mechanical systems. Application to bolted structures. *Journal of Sound and Vibration*, 329:4048–4067, 2010.
14. N. Coudeyras, J. J. Sinou, and S. Nacivet. A new treatment for predicting the self-excited vibrations of nonlinear systems with frictional interfaces: The Constrained Harmonic Balance Method, with application to disc brake squeal. *Journal of Sound and Vibration*, 319(3):1175–1199, January 2009.
15. Guillaume Vermot Des Roches and Etienne Balmes. Understanding friction induced damping in bolted assemblies through explicit transient simulation. In *ISMA*, page ID360. KUL, September 2014.
16. *Structural Dynamics Toolbox (for Use with MATLAB)*. SDTools, Paris, 1995/2020.
17. Michael Feldman. Hilbert transform in vibration analysis. *Mechanical Systems and Signal Processing*, 25(3):735–802, April 2011.